Association of Optic Nerve Head Prelaminar Schisis With Glaucoma

EUGENE A. LOWRY, STEVEN L. MANSBERGER, STUART K. GARDINER, HONGLI YANG, FACUNDO SANCHEZ, JUAN REYNAUD, SHABAN DEMIREL, CLAUDE F. BURGOYNE, AND BRAD FORTUNE

• PURPOSE: To compare the frequency of observing optic nerve head (ONH) prelaminar schisis by optical coherence tomography (OCT) in glaucoma and glaucoma suspect (GL/S) eyes vs healthy control (HC) eyes and to assess its association with other markers of glaucoma severity.

• METHODS: This cross-sectional study included 298 eyes of 150 GL/S patients and 88 eyes of 44 HCs. OCT scans were obtained, including 24 radial B-scans, each composed of 768 A-lines spanning 15°, centered on the ONH. Two reviewers masked to all other clinical, demographic, and ocular information independently graded the OCT scans for the presence of ONH prelaminar schisis on a 4-point scale of 0 (none) to 3 (severe). The probability of ONH schisis was compared between groups and against demographic and ocular factors, including structural and functional measures of glaucoma severity.

• RESULTS: The frequency and severity of ONH prelaminar schisis were greater in GL/S than in HC ($P = .009$). Among the GL/S group, 165 eyes (55.4%) had no visible schisis (Grade 0), 71 (23.8%) had Grade 1, 46 (15.4%) had Grade 2 and 16 (5.4%) had Grade 3 schisis. Among HC eyes, 59 (67.0%) had Grade 0, 24 (27.3%) had Grade 1, 5 (5.7%) had Grade 2, none had Grade 3. ONH schisis was more common in eyes with thinner MRW and a deeper cup.

• CONCLUSIONS: ONH prelaminar schisis may be a sign of glaucomatous deformation and reflect ongoing pathophysiological damage. ONH prelaminar schisis can impact OCT image segmentation and diagnostic parameters, resulting in substantial overestimation of the true rim tissue thickness and underestimation of cup depth. (Am J Ophthalmol 2021;223:246–258.

Accepted for publication Oct 27, 2020.

From the Discoveries in Sight Research Laboratories (E.A.L., S.L.M., S.K.G., H.Y., F.S., J.R., S.D., C.F.B., B.F.), Optic Nerve Head Research Laboratory (H.Y., J.R., C.F.B.), Devers Eye Institute, Legacy Research Institute, Legacy Health, Portland, Oregon, USA.

Inquiries to Brad Fortune, Discoveries in Sight Research Laboratories, Devers Eye Institute and Legacy Research Institute, 1225 NE Second Avenue, Portland, OR 97232, USA; e-mail: bfortune@deverseye.org

THE OPTIC NERVE HEAD (ONH) IS CONSIDERED TO BE the primary site of damage to retinal ganglion cell axons in glaucoma.[1–3] Indeed, the clinical appearance of the ONH in glaucoma is unique among optic neuropathies in that it generally manifests a greater degree of "cupping" and "excavation" for a given severity of vision loss and/or axon loss, which is thought to result from deformation and remodeling of the major load-bearing connective tissues within and surrounding the ONH (the lamina cribrosa and peripapillary sclera).[3–5] The distinct clinical appearance observed in glaucoma serves as an important diagnostic sign by which to differentiate it from other optic neuropathies.[4,6,7]

These ONH conformational changes exist along a spectrum throughout all stages of glaucoma and are often the underlying basis for considering some eyes (or persons) to be "glaucoma suspect" (eg, glaucomatous appearance of the ONH without detectable visual field loss). Longitudinal change of the ONH toward an increasingly glaucomatous appearance is known to be a strong risk factor for subsequent development of glaucomatous visual field loss, that is, for conversion from suspect to manifest glaucoma.[8,9] Thus, even during early stages of glaucoma, the mechanical stresses thought to be driving deformation and remodeling of the ONH are also likely exerting mechanical and physiological stress and on adjacent tissues, perhaps compounded by the ONH conformational changes themselves. For example, we recently reviewed an array of findings from optical coherence tomography (OCT) studies, which demonstrated anatomic disruption within the retina of glaucomatous eyes, sometimes several millimeters from the ONH.[10] One potential explanation we proposed is that the mechanical forces driving ONH deformation and remodeling (eg, in glaucoma and myopia), along with the resulting conformational changes themselves, exert an impact on distant tissue via the retinal blood vessels, internal limiting membrane (ILM), and macroglia (Müller cells).[10] In that review article, we also reported several cases in which the ONH prelaminar tissue had exhibited OCT signs of "schisis" or splitting in association with variants of retinal anatomic disruption in glaucomatous eyes, such as peripapillary retinoschisis and paravascular defects.[10]

Although it will likely be informative to eventually determine whether there is an association between those (or other) retinal abnormalities and the ONH prelaminar

  0002-9394
https://doi.org/10.1016/j.ajo.2020.10.021

schisis sign, it is more immediately important to determine if ONH prelaminar schisis occurs more frequently in glaucomatous eyes than in healthy eyes and whether its presence and/or apparent severity is associated with the degree of glaucomatous damage. Therefore, the purpose of this study was to compare the frequency of observing ONH prelaminar schisis by OCT in glaucoma and glaucoma suspect eyes vs healthy control eyes and to assess the association between ONH prelaminar schisis and other markers of glaucoma severity. Clinicians and researchers would use this information to better understand the spectrum of anatomic and pathologic changes in the glaucoma, and to recognize how prelaminar schisis may influence the OCT evaluation of glaucoma.

METHODS

• **PARTICIPANTS:** This study was conducted using data obtained from 2 groups of participants tested at the Devers Eye Institute in Portland, OR. The healthy control group consisted of 44 adults (88 healthy control eyes) who had been screened by complete ocular examination at the Devers Eye Institute and enrolled in a separate multicenter study designed to establish normative reference ranges for diagnostic OCT parameters used in commercial instrumentation.[11,12] This group thus represents a subset of the individuals comprising the white normative database described in detail in other reports.[11,12] The second group is composed of participants enrolled in the ongoing Portland Progression Project ("P3"), a prospective longitudinal study whose aims include identification of risk factors for glaucoma progression and predictors of its rate.[13] All aspects of this study adhered to the tenets of the Declaration of Helsinki, were approved and monitored by the Legacy Health Institutional Review Board, and are compliant with the Health Insurance Portability and Accountability Act of 1996 (HIPAA). All participants provided written informed consent once all of the risks and potential benefits of participation were explained to them.

At enrollment into the P3 study, all participants had either a clinical diagnosis of early-stage primary open-angle glaucoma, or their physician had determined that they had an optic disc appearance suspicious for glaucomatous optic neuropathy (large cup-to-disc ratio, cup-to-disc asymmetry ≥0.2 between eyes, rim notching, nerve fiber layer thinning or defect, or history of disc hemorrhage) and at least 1 other risk factor for glaucoma (eg, ocular hypertension with documented intraocular pressure ≥22 mm Hg on at least 2 occasions and/or first-degree family history of primary open-angle glaucoma). We also excluded participants from enrolling if visual acuity was worse than 20/40 in either eye and/or if there were any indicators of other ocular diseases or medications that could lead to changes in visual acuity or visual fields. Since their initial enrollment into the longitudinal P3 study, some eyes have progressed to develop worse glaucoma, yet many are still considered by their referring physicians to be glaucoma suspects. Thus, herein we refer to this group of eyes using the abbreviation GL/S. All participants had a complete ophthalmic examination of both eyes including measurement of visual acuity, slit lamp evaluation of the anterior segment, manifest refraction, gonioscopy, pachymetry, and evaluation of the ocular fundus, including optic disc and macula.

To be included in the Healthy Control group, all the following inclusion criteria were required: age between 18 and 90 years; clinically normal eye examination without clinically significant vitreoretinal or choroidal disease or prior intraocular surgery except cataract or refractive surgery; intraocular pressure ≤21 mm Hg; best-corrected visual acuity ≥20/40; refractive error within 6-diopter (D) spherical error and 2 D astigmatic error; normal visual field with both the glaucoma hemifield test and mean deviation (MD) being within normal limits.[11,12]

• **VISUAL FIELD TESTING:** Standard visual field testing was performed using a Humphrey field analyzer (HFA II; Carl-Zeiss Meditec, Dublin, California, USA) with a size III stimulus, SITA standard algorithm, and 24-2 test pattern. All visual field tests included in this study were considered reliable, with fewer than 20% false positives and fewer than 33% fixation losses. We used the visual field glaucoma hemifield test results along with the global indices MD and pattern standard deviation to evaluate associations between the severity of glaucomatous visual field loss and the presence or severity of ONH schisis.

• **OCT IMAGING:** All OCT scans were obtained using a Spectralis instrument (Heidelberg Engineering, GmbH, Heidelberg, Germany) on the same day as visual field testing. The scan pattern was composed of 24 radially oriented B-scans and 3 circumpapillary B-scans as selected from the "ONH-RC" preset available within the instrument's Glaucoma Module Premium Edition. During acquisition for each eye in real time, the scan pattern is centered over the ONH and rotated into alignment with the fovea using the instrument's proprietary Anatomic Positioning System. This system relies on an interactive routine whereby the operator identifies the position of the Bruch membrane opening (BMO) and the base of the foveal pit, each within a pair of live, orthogonal B-scans. Thus, the axis between the fovea and the BMO centroid (the FoBMO axis) defines the "temporal" position (at 0°) of the pattern. The ONH radial B-scans were equally spaced 7.5° apart; each contained 768 A-lines and spanned 15° laterally (approximately 4.4 mm in an "average" adult human eye). For this study, we used only the innermost of the 3 circular B-scans, which had a diameter of 12° (approximately 3.5 mm) and contained 768 A-lines. The number of B-scan sweeps averaged to obtain the final recording in

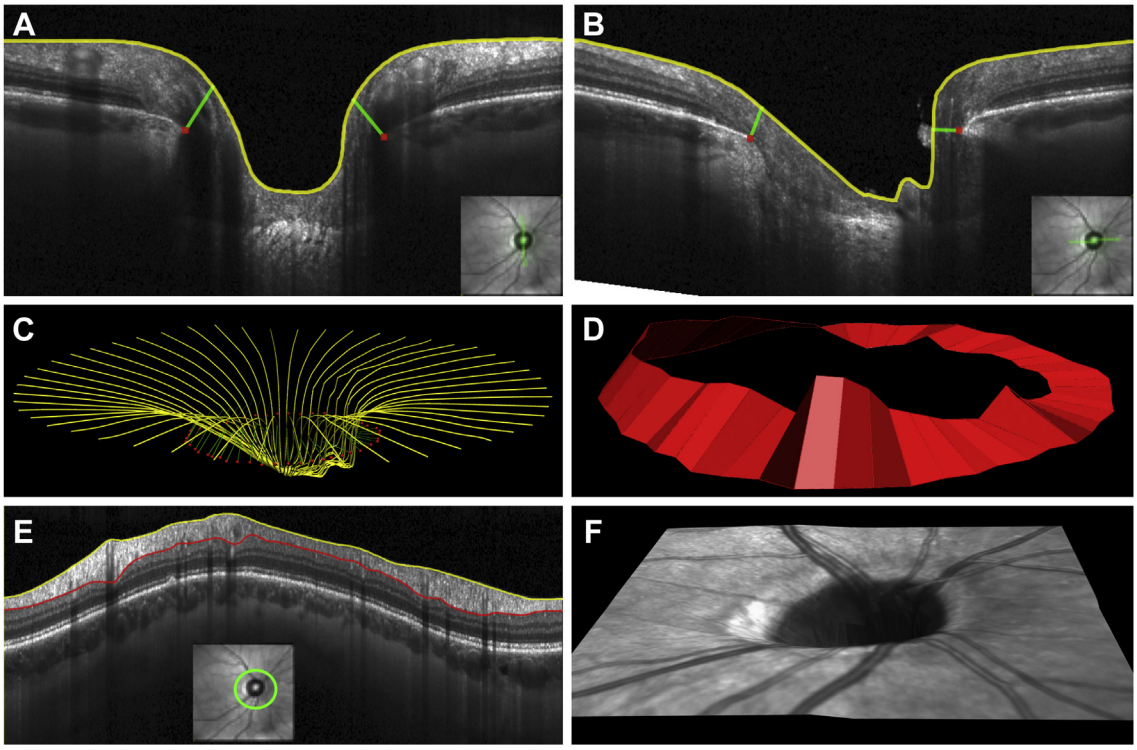

FIGURE 1. Example of an individual GL/S eye from the P3 study group demonstrates methods used to quantify parameters from OCT scans. A. OCT B-scan through the vertical meridian of the ONH (orthogonal to the FoBMO axis). The inset shows the B-scan location indicated by the bold green line overlaid onto the corresponding infrared reflectance image. Structures delineated in each of the 24 radial B-scans include the ILM (yellow contour) and BMO points (red dots). The green line segments connecting BMO points to the ILM represent the minimum distance from each BMO point to the ILM, that is, the pair of MRW vectors determined for each B-scan. B. B-scan through the horizontal meridian of the ONH (along the FoBMO axis); note that the MRW angle is shallow on the nasal (right) side. C. ILM and BMO delineations for all 24 radial B-scans shown from the perspective looking toward the inferior pole of the ONH. D. The parameter MRA was derived as the sum of the 48 radial trapezoidal sectors shown as a red, ribbon-like structure from the same perspective (looking toward the inferior pole of the ONH); note that the MRA angle is shallow along the nasal rim. E. Corresponding circumpapillary B-scan showing delineations of ILM (yellow contour) and posterior RNFL boundary (red contour). F. Infrared reflectance image captured during the OCT scan has been laid onto the ILM surface to provide a clinical view of the surface topography in this eye; it is shown from the same perspective as the 3-dimensional MRW and MRA representations in panels C and D, respectively; the view is toward the inferior pole of the ONH (temporal sector to the left, nasal to the right). Female, age = 62 years; visual field mean deviation = 1.7 dB, pattern standard deviation = 1.2 dB, glaucoma hemifield test = within normal limits; BMO area = 1.99 mm^2; MRW = 261 μm; MRW angle = 34°; MRA = 1.12 mm^2; mean cup depth = 385 μm; maximum cup depth = 399 μm; RNFL thickness = 110 μm; scan quality score = 32.6. BMO = Bruch membrane opening, GL/S = glaucoma suspect, ILM = internal limiting membrane, MRA = minimum rim area, MRW = minimum rim width, OCT = optical coherence tomography, ONH = optic nerve head, RNFL = retinal nerve fiber layer.

each case was predetermined by the automatic real time mean setting of 25 for ONH radial scans and 100 for the circumpapillary B-scan. All OCT scans had a quality score >20.

OCT image segmentations were inspected by the operator on completion of scan acquisition and corrected manually if necessary.[14] For the quantitative analyses applied in this study, we required accurate delineation of 2 image features within the ONH radial B-scans and 2 image features within each of the circumpapillary B-scans, as shown in Figure 1, A, B, and E, respectively. For radial scans, the inner limiting membrane (ILM; yellow contours in Figure 1, A through C) and BMO (red dots in Figure 1, A through C) were used as described below.

Figure 1, A and B, respectively, show a vertically oriented B-scan through the ONH (orthogonal to the FoBMO axis) and a horizontally oriented B-scan (along the FoBMO axis). The pair of green line segments in each B-scan shown in Figure 1, A and B, represent the shortest distance from the BMO point to the ILM segmentation, that is, defining the parameter minimum rim width (MRW). Figure 1, C, shows projected 3D representations of the ILM and BMO for all 24 delineated B-scans viewed from the inferior sector of this example right eye from a P3 participant (with the

temporal sector toward the left). The 48 MRW vectors (green line segments) are also shown. For this study, we averaged these 48 MRW samples in each eye to obtain the global average MRW parameter. MRW angle was defined as 0° when a vector points inward on the BMO plane and as 90° when it points anteriorly (upward in the image), perpendicular to the BMO plane; the average MRW angle for each eye was used for this study.

The ONH minimum rim area (MRA) parameter was derived by summing the areas of each of the 48 trapezoids whose base is 7.5° wide, centered on a BMO point, and whose height is the distance to the ILM segmentation that minimizes its area.[15] The collection of these trapezoids is shown as the red, ribbonlike structure in Figure 1, D, also from a perspective looking toward the inferior pole of the ONH. MRA angle is defined in the same way as MRW angle. This eye has a very shallow MRW and MRA angle (approaching 0°) along the nasal rim.

The corresponding circumpapillary B-scan for this eye is shown in Figure 1, E, with segmentations for the ILM (yellow contour) and the posterior boundary of the retinal nerve fiber layer (RNFL, red contour). The parameter RNFL thickness (RNFLT) used in this study represents the global average thickness (of all 768 samples).

Additional parameters used in this study were derived from the 3-dimensional (3D) fit of an ellipse (via minimization of root mean square error) to the 48 delineated BMO points. BMO area represents the area of that ellipse; BMO nonplanarity was calculated as the standard deviation of axial distances between each BMO point and the fitted ellipse; BMO aspect ratio was calculated as the ratio of the long axis to the short axis of that ellipse. The parameter mean cup depth represents the average axial depth of all ILM samples within the BMO, referenced to the top of the rim (because that reference provides a measure of cup depth that is more independent of rim thickness as compared with using the BMO plane; Supplemental Figure 1). The parameter maximum cup depth represents the most posterior sample of the ILM segmentation within the BMO; its value was referenced to the 3D BMO plane (such that a positive value indicates that none of the ILM samples were posterior to the BMO plane). In this case, the 3D-determined BMO plane provides a more precise estimate against which to reference the single-most posterior voxel within the cup (vs the much larger nonplanarity of the rim).

• **GRADING ONH PRELAMINAR SCHISIS IN OCT SCANS:** For GL/S eyes (in which OCT scans are obtained every 6 months), we graded the most recently available scans. In all eyes, the same OCT scans used for grading of ONH prelaminar schisis were also used for quantification of structural parameters. Two graders (E.A.L. and B.F.) independently reviewed the ONH OCT scans (24-radial B-scans) for each eye in the study via the Display tab of the instrument's user interface. Graders were masked to all patient demographic, clinical, and ocular information, including visual field results and quantitative parameters from the OCT scans, as well as to each other's grades. A 4-point scale (zero to 3) was used for grading the severity of ONH schisis in each eye, which corresponded essentially to 0 = none, 1 = mild, 2 = moderate, and 3 = severe (see Figures 2 and 3). Specifically, the lateral boundary defining the ONH for the purpose of grading was the pair of BMO points within each B-scan: Grade 1 was applied when the size of the apparent optical void or voids were relatively small and located within the anteriormost portion of the ONH prelaminar tissue (ie, just beneath the surface); Grade 2 was applied to eyes in which the schisis was larger and/or located deeper within the prelaminar tissue (because schisis at deeper locations implies disruption of axoglial tissue architecture); Grade 3 was applied to eyes in which the schisis volume was much larger in size (eg, within a given B-scan and/or visible in many more B-scans) and associated with definite disruption of the subsurface ONH prelaminar tissue (Figure 2). Graders also noted whether or not there was clear evidence of vitreous adhesions to the ONH surface (ie, within the BMO boundary) and whether or not there was evidence of posterior vitreous cortex adhering to the peripapillary retina and/or that the peripapillary ILM was lifted away from underlying retina (see Figures 2 and 3). There was good agreement between the 2 graders' initial scores, with identical scoring of 272 eyes (70.5%) and scores within 1 point in 373 eyes (96.6%). Overall, there was substantial agreement between the 2 graders for schisis vs no schisis (kappa = 0.66, 95% confidence interval: 0.58-0.73) and for the specific schisis grade (weighted kappa = 0.62). Among the 114 (of 386) eyes for which there was an initial difference between graders, the vast majority (95 of 114, 83%) were in the GL/S group, and most of those differed by only 1 level (87 of 95, 92%). OCT scan quality score was not a significant influence on the initial intergrader differences (P = .180), probably because the scan quality score was higher than 20 in all eyes (Table 1). Subsequently, all disagreements between graders were reconciled by consensus to achieve a final grade for each eye; graders remained masked to all other information during the consensus process.

• **ANALYSIS AND STATISTICS:** Statistical analysis was performed using either a commercial software package (Prism 8; GraphPad Software, Inc, La Jolla, California, USA) or the R language and environment for statistical computing (R, version 3.3.3; R Core Team, Vienna). Differences between study groups were evaluated using either an unpaired, 2-sided t test with Welch correction for continuous variables such as visual field indices and OCT parameters or by Fisher exact test for binary variables. To evaluate associations between ONH schisis and each of the potential predictors, 2 sets of analyses were performed. First, logistic models were used to predict the odds of the

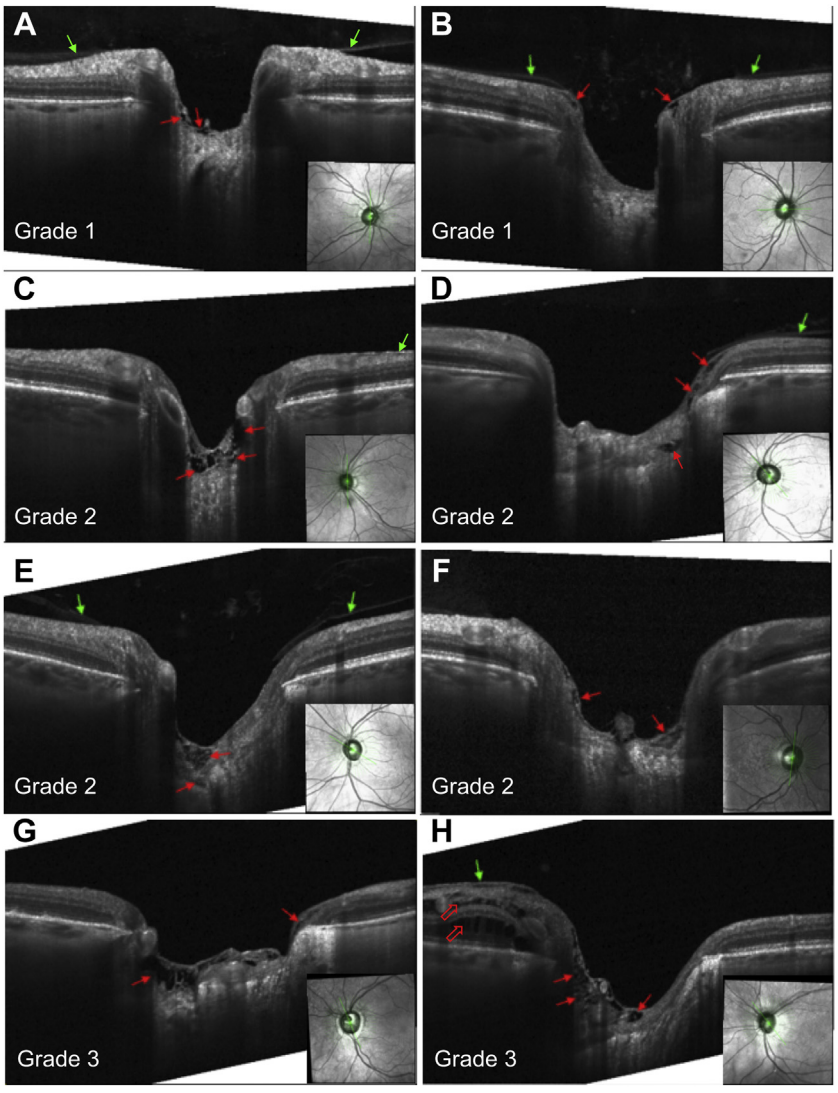

FIGURE 2. Examples of ONH prelaminar schisis in GL/S eyes. Each panel contains one of the ONH OCT radial B-scans of a GL/S eye from the P3 study group; the radial orientation of the B-scan is indicated by the bold green line in the inset at the lower right corner of the panel (as in Figure 1). Red arrows point to optical voids whose size and depth were used to determine severity grade of ONH schisis. Green arrows point to locations where the peripapillary ILM appears to be separated from the underlying RNFL tissue. Open red arrows point to peripapillary retinoschisis. GL/S = glaucoma and glaucoma suspect, ILM = internal limiting membrane, OCT = optical coherence tomography, ONH = optic nerve head, RNFL = retinal nerve fiber layer. Panel labels A–H are referenced in the main text.

detection of any ONH schisis (ie, scores 1, 2, or 3, vs score 0), using a generalized estimating equation framework to account for the presence of fellow eyes in the data set. Second, proportional odds ordinal logistic regression models were used to predict the actual score (ie, making the implicit assumption that the effect of a predictor on the odds of being score 1 vs. score 0 exactly equals the effect on the odds of being score 2 vs score 1, or of being score 3 vs score 2); using robust sandwich estimates of the standard errors to account for the presence of fellow eyes. In each case, various potential predictors of ONH schisis were evaluated univariately. Predictors that had a univariate $P < .2$ were then entered into a multivariable model, and a final model was derived by single backward elimination. All other statistical analyses are listed in context with presentation of corresponding results in the next section.

RESULTS

TABLE 1 LISTS THE DEMOGRAPHIC CHARACTERISTICS, VISUAL field, and OCT structural parameters measured in the 2 study groups. As expected, there were substantial differences between the GL/S group and the healthy control group for parameters reflecting glaucomatous visual field and

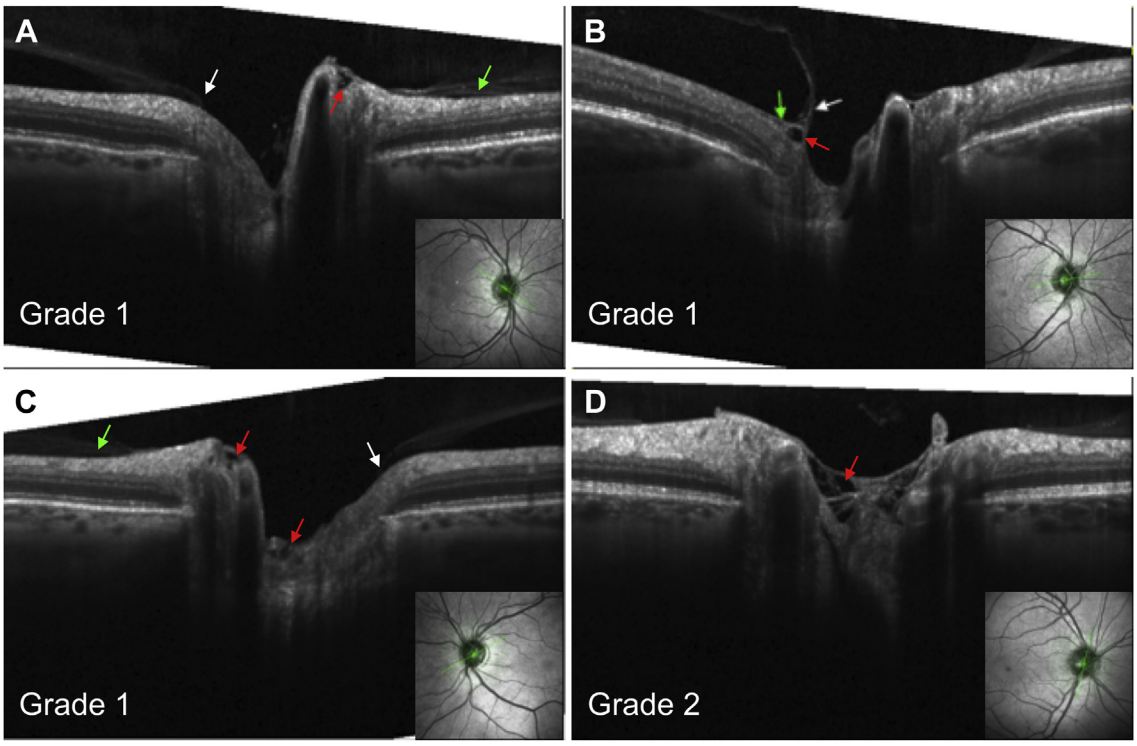

FIGURE 3. Examples of ONH prelaminar schisis in eyes of the healthy control group. Each panel contains one of the ONH OCT radial B-scans of an eye from the healthy control group; the radial orientation of the B-scan is indicated by the bold green line in the inset at the lower right corner of the panel (as in Figures 1 and 2). Red arrows point to optical voids whose size and depth were used to determine severity grade of ONH schisis. Green arrows point to locations where the peripapillary ILM appears to be separated from the underlying RNFL tissue. White arrows point to locations where the vitreous appears adherent to the ONH tissue. ILM = internal limiting membrane, OCT = optical coherence tomography, ONH = optic nerve head, RNFL = retinal nerve fiber layer. Panel labels A–D are referenced in the main text.

structural damage: visual field indices MD and pattern standard deviation and the frequency of glaucoma hemifield test being abnormal, as well as the OCT parameters MRW, MRW angle, MRA, mean cup depth, maximum cup depth, and circumpapillary RNFL thickness (all $P < .0001$). In addition, the OCT parameter BMO area was 16% larger in GL/S eyes, on average, than in healthy control eyes ($P < .0001$); BMO aspect ratio was slightly smaller (ie, BMO was rounder, or less oval; $P = .001$) and the BMO tended toward greater nonplanarity ($P = .08$) in GL/S eyes. The frequency of observing either vitreous adhesions to the ONH surface or separation ("lift") of the peripapillary ILM was higher in healthy control eyes (each $P < .0001$). Although participants in the GL/S group were 20 years older, on average, than the healthy controls ($P < .0001$), their OCT scan quality score tended to be slightly better ($P = .07$).

The frequency and severity of ONH prelaminar schisis were greater in GL/S eyes than in healthy controls ($\chi^2 = 11.54$, $P = .009$; Figure 4). Among the GL/S group, 165 eyes (55.4%) had no visible schisis (Grade 0), 71 (23.8%) had Grade 1, 46 (15.4%) had Grade 2, and 16 (5.4%) had Grade 3 schisis. Among the healthy control eyes, 59 (67.0%) had Grade 0, 24 (27.3%) had Grade 1, 5 (5.7%) had Grade 2, and none of the healthy control eyes had Grade 3 schisis. The optical voids defining the OCT appearance of ONH schisis were generally larger and located deeper into the prelaminar ONH tissue, resulting in a more disrupted appearance of the tissue architecture in the GL/S eyes as compared to healthy control eyes (eg, Figures 2 and 3).

Figure 5 shows the distribution of visual field and OCT parameters by study group and ONH schisis grade. The array of plots in Figure 5 reveal several parameters that appear to have a strong association with ONH schisis severity. For example, ONH schisis grade exhibits a clear association with MRW (Figure 5, G), MRW angle (Figure 5, H), and mean cup depth (Figure 5, I), driven largely by the group of GL/S eyes, whereas the association with other parameters such as BMO area (Figure 5, D) and maximum cup depth (Figure 5, L) appears to manifest in both GL/S and Healthy Control eyes. In contrast, although some parameters such as age and circumpapillary RNFL thickness show a clear difference between the GL/S and Healthy Control groups, there is not much association with ONH schisis apparent in either group. Specifically, there was no significant difference in age between control eyes grouped by ONH schisis grade (Grade 0, 1, or 2; $P = .483$; 1-way analysis of variance), nor between the 4 groups of GL/S eyes (Grade 0, 1, 2, or 3; $P = .300$).

TABLE 1. Demographic and Ocular Characteristics of the 2 Study Groups: Glaucoma/Suspects and Healthy Controls

	Glaucoma/Suspect 298 Eyes of 150 Persons		Healthy Controls 88 Eyes of 44 Persons		
Parameter	Mean ± SD	Range	Mean ± SD	Range	*P* Value
Age, y	72.2 ± 9.0	48.8-94.0	52.6 ± 17.4	22.3-84.4	<.0001[a]
Gender	62 Male (41%)/ 88 Female (59%)		19 Male (43%)/ 25 Female (57%)		.863[b]
Abnormal or borderline GHT	113 (38%)		0 (0%)		<.0001[b]
MD, dB	−1.19 ± 3.65	−20.74 to 2.83	0.28 ± 0.87	−1.52 to 2.08	.005[c]
PSD, dB	2.95 ± 2.89	0.97-15.11	1.43 ± 0.26	0.94-2.65	<.0001[c]
BMO area, mm^2	2.00 ± 0.44	1.07-3.40	1.72 ± 0.31	1.15-2.45	<.0001[c]
BMO nonplanarity, μm	22.2 ± 9.3	5.7-78.2	20.3 ± 8.7	8.1-67.5	.053[c]
BMO aspect ratio	1.11 ± 0.06	1.01-1.32	1.14 ± 0.07	1.01-1.33	.001[c]
MRW, μm	240.8 ± 67.9	56.0-416.6	348.0 ± 63.4	236.1-549.3	<.0001[c]
MRW angle, degrees	50.5 ± 15.5	11.7-81.6	64.6 ± 9.9	35.5-81.3	<.0001[c]
MRA, mm^2	1.06 ± 0.28	0.27-1.89	1.36 ± 0.23	0.85-2.10	<.0001[c]
MRA angle, degrees	37.0 ± 11.6	12.8-69.4	36.1 ± 10.8	19.4-71.0	.398[c]
RNFLT, μm	82.7 ± 17.0	27.8-131.3	96.7 ± 10.6	63.1-121.2	<.0001[c]
Mean cup depth, μm	314.6 ± 120.9	78.7-723.7	222.3 ± 84.6	23.9-450.1	<.0001[c]
Max cup depth, μm	334.5 ± 185.1	−137.5 to 891.5	171.5 ± 200.1	−263.6 to 613.3	<.0001[a]
Scan quality score	30.2 ± 3.2	21.3-39.7	29.5 ± 3.4	20.8-38.4	.042[c]
Vitreous-to-ONH	78 (26.2%)		43 (48.9%)		<.0001[b]
Peripapillary ILM lift	112 (37.6%)		67 (76.1%)		<.0001[b]

Standard automated perimetry visual field parameters: glaucoma hemifield test (GHT); mean deviation (MD); and pattern standard deviation (PSD). Optical coherence tomography (OCT) parameters: Bruch membrane opening (BMO); minimum rim width (MRW); minimum rim area (MRA); retinal nerve fiber layer thickness (RNFLT); optic nerve head (ONH); and internal limiting membrane (ILM).

[a]Welch *t* test.

[b]Fisher exact test.

[c]Mann-Whitney *t* test.

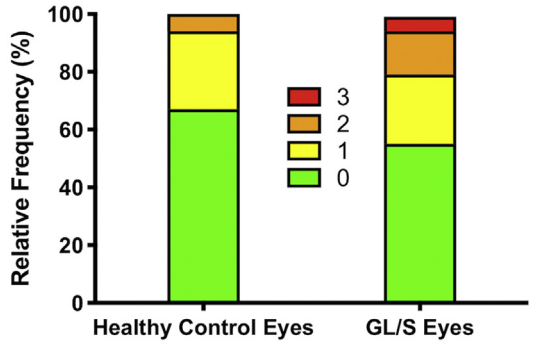

FIGURE 4. Frequency and severity of ONH prelaminar schisis in each study group. Stacked frequency histogram shows that ONH prelaminar schisis was observed more frequently and had higher severity grades among the GL/S group as compared to the healthy control group ($\chi^2 = 11.54$, $P = .009$; color indicates schisis grade). GL/S = glaucoma suspect, ONH = optic nerve head.

To formally evaluate the association between ONH prelaminar schisis and each of these potential predictors, we used 2 types of logistic models (as detailed above in Methods). Table 2 shows the effect of each potential predictor in 2 types of univariate analyses. The first set of logistic models were used to predict the odds of detecting any ONH schisis (ie, score of 1, 2, or 3 vs score of 0); the second set of proportional odds ordinal logistic regression models were used to predict the actual schisis score. The 2 types of analysis returned very similar results, consistent with the findings presented in Figure 5. The frequency and severity grade of ONH prelaminar schisis exhibited significant associations with several common clinical measures of glaucomatous damage; OCT parameters reflecting glaucomatous deformation of the ONH, in particular, MRW, MRW angle, mean and maximum cup depth appear to be the most robust predictors of ONH schisis being present and being more severe.

Starting with the variables that achieved $P < .2$ in the univariate models shown in the final column of Table 2, we created a multivariable proportional odds ordered logistic model to predict ONH schisis grade. To minimize the effects of instability due to collinearity, the MRW and MRW angle were included but MRA and MRA angle omitted (because the MRW parameters showed slightly stronger relations to schisis than the MRA parameters, likely due to MRW being less variable than MRA), and with maximum cup depth used but mean cup depth omitted

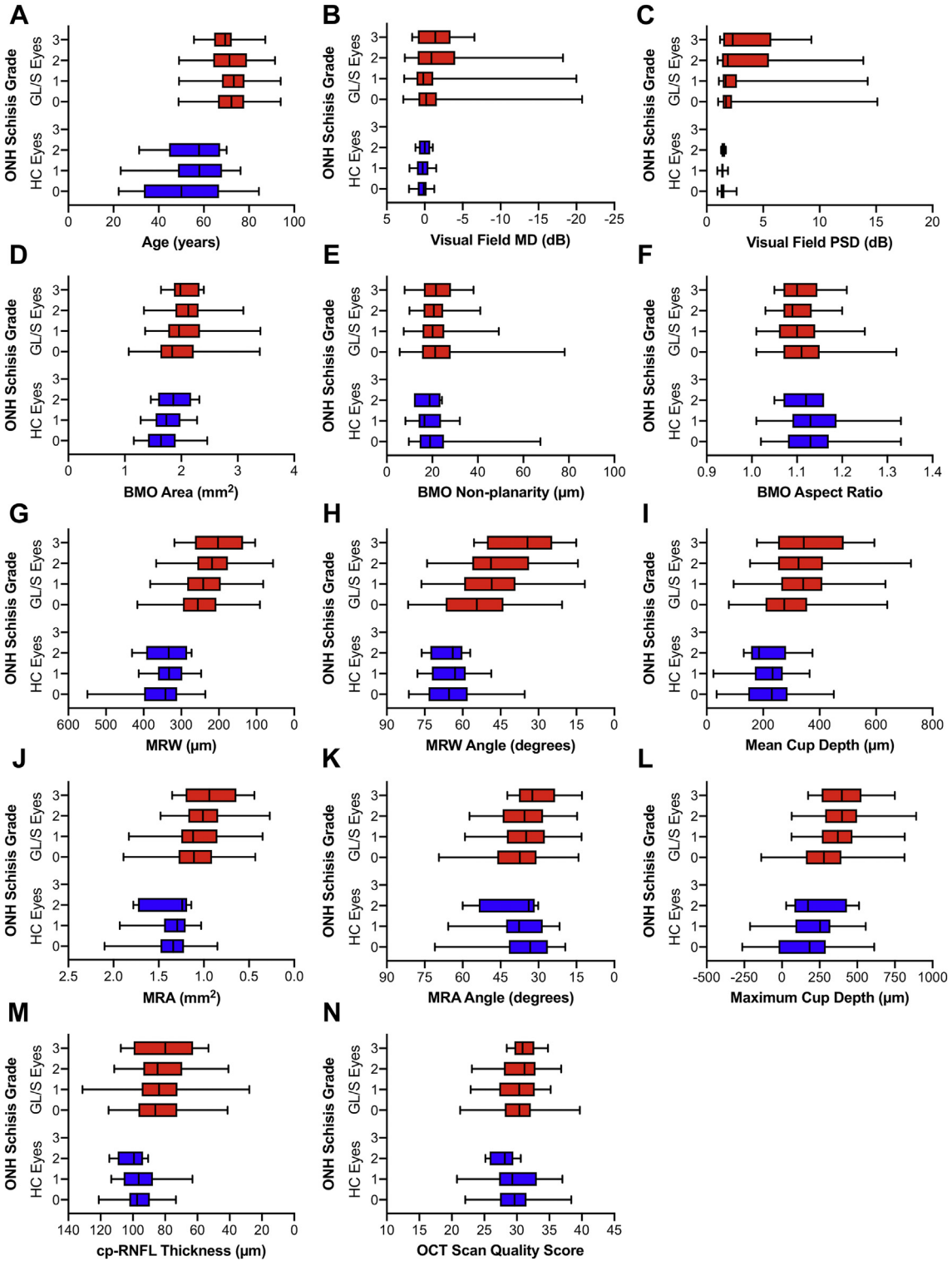

FIGURE 5. Distribution of visual field and OCT parameters by study group and ONH schisis grade. Box plots represent the median, interquartile range and extremes of each distribution. The healthy control group (HC) is shown in blue and the glaucoma/suspect (GL/S) group in red. ONH prelaminar schisis grade plotted versus each parameter as follows: (A) age; (B) visual field mean deviation (MD); (C) visual field pattern standard deviation (PSD); (D) Bruch's membrane opening (BMO) area; (E) BMO non-planarity; (F) BMO aspect ratio; (G) ONH minimum rim width (MRW); (H) MRW angle; (I) mean cup depth; (J) ONH minimum rim area (MRA); (K) MRA angle; (L) maximum cup depth; (M) circumpapillary retinal nerve fiber layer (cp-RNFL) thickness; (N) OCT scan quality score. OCT = optical coherence tomography, ONH = optic nerve head.

TABLE 2. The Effect of Each Predictor in Univariate Analyses

Predictor	Increment	Odds Ratio	*P* Value	Odds Ratio	*P* Value
Group	In the P3 group	1.64 (0.90-2.98)	.10	1.88 (1.17-3.08)	.02
Age	10 y older	1.16 (0.98-1.37)	.09	1.15 (1.00-1.33)	.09
Abnormal GHT	Abnormal or borderline	1.80 (1.13-2.88)	.01	1.87 (1.23-2.85)	.009
MD	1 dB more negative	1.07 (0.99-1.15)	.07	1.07 (1.02-1.14)	.03
PSD	1 dB more positive	1.12 (1.01-1.23)	.03	1.12 (1.05-1.20)	.008
BMO area	0.1 mm^2 larger	1.07 (1.02-1.14)	.01	1.07 (1.03-1.12)	.005
BMO nonplanarity	1 μm smaller	1.03 (0.99-1.04)	.19	1.01 (0.99-1.04)	.26
BMO aspect ratio	0.1 units smaller	1.23 (0.85-1.77)	.27	1.26 (0.92-1.75)	.17
MRW	10 μm smaller	1.06 (1.03-1.09)	.0001	1.07 (1.04-1.10)	<.0001
MRW angle	1° smaller	1.04 (1.02-1.05)	<.0001	1.04 (1.03-1.05)	<.0001
MRA	0.1 mm^2 smaller	1.10 (1.02-1.19)	.02	1.13 (1.05-1.21)	.003
MRA angle	1° smaller	1.02 (1.00-1.04)	.09	1.02 (1.00-1.04)	.06
RNFLT	1 μm smaller	1.01 (1.00-1.03)	.17	1.01 (1.00-1.02)	.11
Mean cup depth	10 μm larger	1.04 (1.02-1.06)	.0003	1.04 (1.02-1.06)	<.0001
Max cup depth	10 μm larger	1.03 (1.02-1.04)	<.0001	1.03 (1.02-1.04)	<.0001
Quality score	1 unit lower	0.99 (0.93-1.06)	.79	0.98 (0.92-1.04)	.57
Vitreous-to-ONH	True	1.17 (0.72-1.90)	.52	1.17 (0.77-1.77)	.52
Peripapillary ILM lift	True	0.91 (0.57-1.47)	.71	0.99 (0.66-1.46)	.95

BMO = Bruch membrane opening, GHT = glaucoma hemifield test, ILM = internal limiting membrane, MD = mean deviation, MRA = minimum rim area, MRW = minimum rim width, OCT = optical coherence tomography, PSD = pattern standard deviation, RNFLT = retinal nerve fiber layer thickness, ONH = optic nerve head.

The second column shows the increment of that predictor used; in each case, the increment is chosen to give the odds ratio for if an eye has a clinically relevant magnitude of worse glaucomatous damage. The third column shows the odds ratio for the presence of schisis (ie, score 1, 2, or 3) compared to no schisis (ie, score 0) when the predictor changes by the stated increment, in a generalized estimating equation logistic regression model (with the associated 95% confidence interval); the fourth column shows the significance of this odds ratio. The fifth column shows the odds ratio from a proportional odds model treating score as an ordered factor variable (together with its confidence interval); the final column shows the significance of this odds ratio.

(by the same logic). After single backward elimination, the final model predicted that ONH schisis grade would be higher in eyes with larger BMO area (odds ratio 1.06 for 0.1 mm^2 larger BMO area, 95% confidence interval 1.01-1.11; $P = .028$) and smaller MRW angle (odds ratio 1.04 for 1-degree smaller angle, 95% confidence interval 1.02-1.05; $P < .0001$); these tend to result in a clinical appearance of having a larger and deeper cup, respectively.

Although age was not a significant predictor of ONH schisis presence or severity in our multivariable analyses after backward elimination, we conducted further analysis retaining age in the multivariable model because the average age of the GL/S and Healthy Control groups differed by 19.6 years (Table 1) and because this age range is commonly when interactions between the vitreous and the ILM can change (such as occurring during posterior vitreous detachment). When we repeated the multivariable analysis retaining age as a predictor in all models, rather than eliminating it via the usual backward elimination process, ONH schisis grade was still predicted by greater BMO area ($P = .031$) and smaller MRW angle ($P < .001$), but not by age ($P = .456$). Similarly, when using MRA instead of MRW, age was not significant in the final model ($P = .882$).

DISCUSSION

HERE WE REPORT THAT ONH PRELAMINAR SCHISIS IS MORE commonly observed in OCT scans of eyes with glaucoma, and that its presence and severity are associated with the severity of glaucomatous damage as measured using a variety of standard clinical diagnostic parameters. This sign should not be considered diagnostic in isolation as mild examples were also found in the healthy control eyes. However, in the vast majority of the healthy eyes, the optical void was small and located just below to the surface, appearing to be separation of the inner limiting membrane of Elschnig and the central meniscus of Kuhnt[16] away from the underlying ONH tissue in a highly localized area (eg, Figure 3). In contrast, in the GL/S eyes, the optical voids were generally much larger and often located deeper within the subsurface ONH tissue. In the most severe examples, the ONH schisis was associated with clear disruption of the deeper prelaminar ONH tissue, and in some cases the tissue disruption appeared to include the lamina cribrosa (eg, Figure 2, G) and peripapillary retina (eg, Figure 2, H). Such examples were never observed in healthy control eyes. These observations may be related to lamina cribrosa

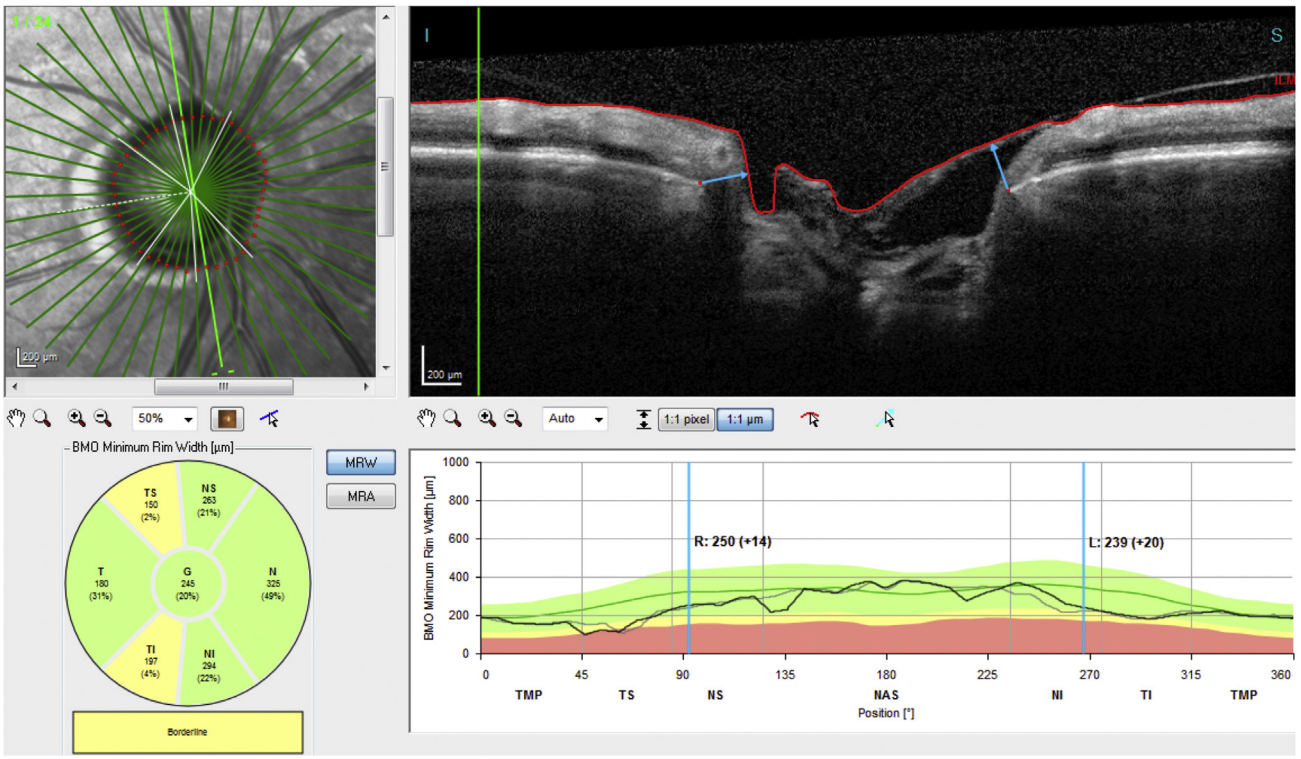

FIGURE 6. Example showing impact of ONH prelaminar schisis on clinical diagnostic parameters. The image shows the clinical instrument report for the MRW parameter in an eye from the GL/S group with a Grade 3 ONH schisis (male, age: 87 years; mean deviation: –6.1 dB; pattern standard deviation: 9.3 dB; RNFLT: 61.0 µm; BMO area 2.01 mm^2; MRW: 221 µm; mean cup depth: 340 µm). A potentially important clinical consequence of ONH schisis is its influence on OCT image segmentation and diagnostic parameters. This example demonstrates how the true MRW values can be dramatically overestimated and cup depth values underestimated. A corollary of this is that our results probably underestimate the association between these parameters and the presence of ONH schisis. BMO = Bruch membrane opening, GL/S = glaucoma suspect, MRW = minimum rim width, OCT = optical coherence tomography, ONH = optic nerve head, RNFLT = retinal nerve fiber layer thickness.

defects in glaucoma detected by OCT[17–19] but are distinctly different insofar as the tissue disruption is within the prelaminar ONH. Isolated case reports or small series have shown similar findings in eyes with optic pit, coloboma, or other cavitary ONH abnormalities,[20,21] including one with coexisting glaucoma,[22] and other examples in glaucoma,[23] but ours is the first systematic study to document the frequency and severity spectrum of this finding in a larger cohort and demonstrate an association with the degree of glaucomatous ONH deformation.

Thus, the presence of a more severe ONH prelaminar schisis should alert clinicians to a higher risk of ongoing glaucomatous damage, as supported by the clear associations we report here for common structural parameters such as ONH size (BMO rea), neuroretinal rim width and cup depth. Although it is not used commonly for clinical diagnostics, the MRW angle parameter also exhibited a strong association with ONH prelaminar schisis and has previously been shown to track closely with ONH deformation in experimental glaucoma.[24] Although prelaminar schisis might reflect ongoing structural change due to glaucomatous deformation and remodeling of the ONH, likely owing to mechanical failure of the load-bearing connective tissues, it is also possible that it represents a risk factor for further damage. Future longitudinal studies are needed to determine if ONH prelaminar schisis is itself predictive of more rapid subsequent glaucoma progression.

Another important clinical implication for ONH prelaminar schisis is its potential to influence diagnostic parameters derived from OCT scans. Figure 6 presents another case example of a Grade 3 ONH schisis in one of the GL/S eyes. The purpose of providing this particular example is 3-fold. First, it demonstrates that ONH schisis can impact the diagnostic parameters and the clinical report produced by the instrument—in this particular case by creating risk of "green disease" whereby the ONH rim thickness (MRW parameter) is reported to be within normal limits for the superior pole despite the true rim thickness being extremely narrow (~50 µm, not 250 µm as reported). Thus, it also serves to reiterate the importance of routinely inspecting the actual B-scans and their

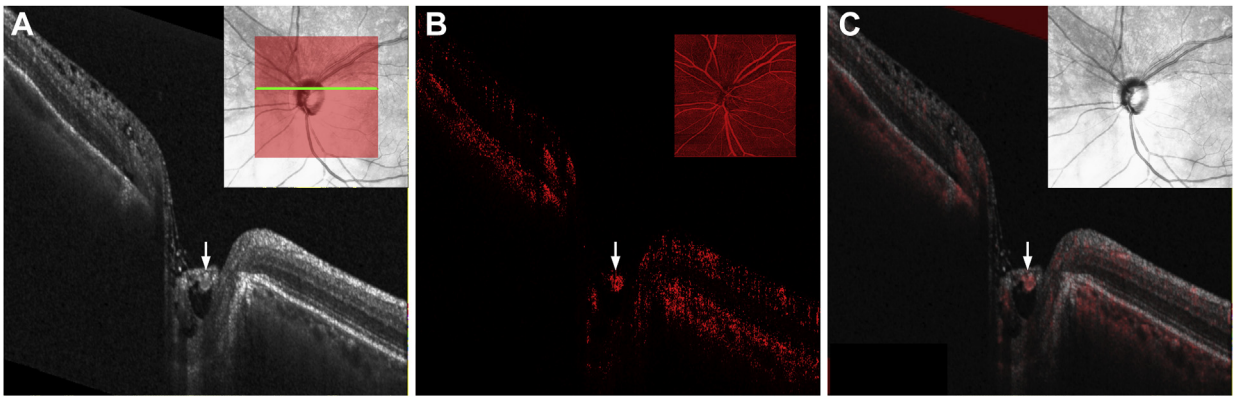

FIGURE 7. Example of OCT angiography demonstrating how the vasculature is involved in some cases of ONH schisis. (A) OCT B-scan whose position is shown by the bright green line within the inset image. (B) Same B-scan showing OCT angiography (OCTA) signal; inset shows the en face projection image for the full depth of the OCTA scan. (C) OCTA B-scan from panel B overlaid with OCT scan from panel A; inset shows the infrared reflectance image. In this eye (the same eye shown in Figure 2, H), major blood vessel trunks are separated anteriorly from the underlying prelaminar tissue (arrow in C); there are strands of presumably connective tissue spanning the optic cup, which appear connected to this vessel. OCT = optical coherence tomography, ONH = optic nerve head.

segmentations to minimize risk of misdiagnosis.[14] Second, it underscores the need for scientists and industry to develop more elaborate and robust segmentation capabilities to account for unusual anatomy, such as exists with ONH prelaminar schisis. Finally, this example also suggests that the strength of cup depth as a predictor of ONH prelaminar schisis might be even greater than we report here because the true cup depth in some cases with higher-grade ONH schisis might be even larger, given that the ILM segmentation generally does not account for the schisis space. To help visualize this scenario, Supplemental Figure 2 shows the ILM and BMO segmentations for the same 8 examples shown earlier in Figure 2.

ONH prelaminar schisis may also have implications for glaucoma pathophysiology. For example, we previously proposed that ONH prelaminar schisis may include detachment of the blood vessels and aspects of their adventitia from the gliofibrillar meniscus of Kuhnt, the ILM of Elschnig, and in some cases also from underlying prelaminar tissue as posterior deformation of the ONH progresses—because the blood vessels are tethered throughout the retina and might thus be limited in how far posteriorly they can be displaced as "cupping" progresses.[10] We surmised this initially from scrutiny of structural OCT scans. However, Figure 7 shows an OCT-angiography scan from an eye with prominent signs of ONH prelaminar schisis. This example clearly demonstrates that major blood vessels are sometimes contained within the strands of tissue separated anteriorly from the underlying prelaminar tissue, a form of "vessel baring" or "bridging" within the ONH rim. In contrast, the major blood vessels are usually embedded within the rim tissue in healthy eyes. Such changes may also have a role in the development of optic disc (Drance) hemorrhages in glaucoma, a topic of study currently underway. Further support for this scenario derives from the observation that major blood vessel cross sections within the ONH rim tissue are rarely ever observed posterior to the BMO in radially oriented OCT B-scans of healthy eyes. In contrast, this is quite commonly observed in eyes with glaucomatous deformation (eg, Figure 2, G). Changes in vessel position, both within the ONH[25,26] and the peripapillary retina,[27] are a well-known sign of glaucomatous deformation and are associated with disease progression. Longitudinal tracking of vessel position may also help determine relationships between glaucomatous ONH changes and development of prelaminar schisis, retinal abnormalities like peripapillary retinoschisis, and paravascular defects.[10]

In addition to the mechanical consequences of glaucomatous ONH deformation and remodeling, there may also be alterations of physiology contributing to failure of homeostasis within the tissue under stress. For example, aquaporin-4 (AQP4) is a water channel thought to be primarily responsible for maintenance of water flux in the retina and optic nerve as evidenced by its highly polarized distribution in Müller glia and astrocytes.[28] Yet it is not expressed by the astrocytes within the prelaminar portion of the ONH in rodents, whereas an entirely different aquaporin channel (AQP9) is instead.[28,29] This suggests some potentially important differences in the way water flux is handled in this highly specialized transition region. Moreover, ONH astrocytes are known to respond rapidly to IOP elevation by retracting and reorienting their processes,[30–34] as well as by exhibiting altered expression of aquaporin channels.[29,35] These changes may be beneficial for some aspects of the response, but the presumed loss of the astrocyte syncytium functions, such as those dependent on end-foot contacts where aquaporin and rectifying potassium channels are normally enriched, might result in reduced capacity to handle ionic and water flux, potentially leading to

fluid accumulations, among other physiological disturbances. This might even further exacerbate mechanical challenges faced by the ONH tissues during glaucomatous deformation and remodeling.

Limitations of this study include that the population is nearly entirely white, which may limit its generalizability. Moreover, the grading scale we used for evaluation of ONH prelaminar schisis was subjective and mostly qualitative. However, we found generally good agreement between graders and reduced the risk of bias by using 2 independent masked observers and a combination of logistic regression approaches for analysis, which produced similar results, thus supporting their robustness. Nevertheless, future studies might benefit from more advanced image segmentation techniques and/or enhanced contrast provided by other imaging modalities, perhaps aided by artificial intelligence, to detect and quantify aspect of ONH schisis objectively. In a similar context, our study used the ONH-RC scan pattern of 24 radials; dense raster scans might increase detection of ONH schisis and improve quantification of size. Moreover, the radial scan pattern samples the central portion of the ONH more densely than the lateral portions where blood vessel shadows more commonly obscure underlying details. Graders tried to account for position within the ONH when considering the size or extent of voids representing ONH schisis, but this was likely one important factor contributing to initial differences between graders.

Additional limitations include that the GL/S group includes relatively few GL eyes with more advanced damage and that the healthy control group was a relatively small sample of only 88 eyes of 44 individuals. This was smaller than the GL/S group and also 20 years younger, on average. However, age was not a significant predictor of ONH prelaminar schisis in a univariate model, nor was age a significant predictor in any of the multivariable models in which it was included, so it is unlikely that the age difference mattered in this regard. Although our results do show a significant association between glaucoma severity and the presence or grade of ONH schisis, this was much stronger for the structural parameters than for visual field indices. For example, the visual field indices were not significant predictors in multivariable models that also included structural predictors, suggesting that glaucomatous structural damage is more strongly associated with ONH schisis (but functional damage less so), or that the measures of function are largely redundant with those of structure. However, only 24 of the 298 GL/S eyes had MD worse than –6 dB, which may be too few to more fully evaluate the relationship between ONH schisis and stage of glaucomatous functional loss. Further work to evaluate larger populations of healthy, glaucomatous, and suspect eyes with more varied ethnicity and a wider range of glaucomatous visual field loss will help to refine and extend our understanding of how ONH schisis develops and to what extent it is related to the stage of glaucomatous damage. Moreover, future longitudinal studies will help determine whether ONH schisis is a consequence of glaucoma progression and/or itself a predictor of future glaucoma progression, as well as whether its appearance changes over time.

In summary, we found that the ONH prelaminar schisis sign was detected more frequently in OCT scans of glaucomatous eyes compared with healthy control eyes and that its presence and severity are associated with common OCT metrics related to increased risk, ONH deformation and structural damage in glaucoma, such as larger ONH size, thinner neuroretinal rim width and greater cup depth.

FUNDING/SUPPORT: THIS WORK WAS SUPPORTED BY THE NATIONAL INSTITUTES OF HEALTH/NATIONAL EYE INSTITUTE (grants: R01-EY020922 [S.K.G.], R01-EY021281 [C.F.B.], R01-EY030590 [B.F.]) and the Legacy Good Samaritan Foundation. These funding organizations had no role in the design or conduct of this research.

Financial Disclosures: S.L.M.: consultant fees from Bausch & Lomb, Santen, New World Medical, Envisia, Gore; Envisia, Alcon, Ocular Therapeutix, and Allergan; S.K.G.: equipment support from Heidelberg Engineering, GmbH; C.F.B.: consultant fees and research support from Heidelberg Engineering, GmbH; B.F.: consultant fees and research Support from Perfuse Therapeutics, Inc, and equipment support from Heidelberg Engineering, GmbH. The other authors indicate no financial support or conflicts of interest. All authors attest that they meet the current ICMJE criteria for authorship.

REFERENCES

1. Emery JM, Landis D, Paton D, Boniuk M, Craig JM. The lamina cribrosa in normal and glaucomatous human eyes. *Trans Am Acad Ophthalmol Otolaryngol* 1974;78(2):290–297.
2. Vrabec F. Glaucomatous cupping of the human optic disk: a neuro-histologic study. *Albrecht Von Graefes Arch Klin Exp Ophthalmol* 1976;198(3):223–234.
3. Quigley HA, Addicks EM, Green WR, Maumenee AE. Optic nerve damage in human glaucoma. II. The site of injury and susceptibility to damage. *Arch Ophthalmol* 1981;99(4):635–649.
4. Burgoyne C. The morphological difference between glaucoma and other optic neuropathies. *J Neuroophthalmol* 2015;35(Suppl 1):S8–S21.
5. Yang H, Reynaud J, Lockwood H, et al. The connective tissue phenotype of glaucomatous cupping in the monkey eye—clinical and research implications. *Prog Retin Eye Res* 2017;59:1–52.
6. Danesh-Meyer HV, Boland MV, Savino PJ, et al. Optic disc morphology in open-angle glaucoma compared with anterior ischemic optic neuropathies. *Invest Ophthalmol Vis Sci* 2010;51(4):2003–2010.
7. Fard MA, Afzali M, Abdi P, et al. Optic nerve head morphology in nonarteritic anterior ischemic optic

neuropathy compared to open-angle glaucoma. *Invest Ophthalmol Vis Sci* 2016;57(11):4632–4640.
8. Medeiros FA, Alencar LM, Zangwill LM, Bowd C, Sample PA, Weinreb RN. Prediction of functional loss in glaucoma from progressive optic disc damage. *Arch Ophthalmol* 2009;127(10):1250–1256.
9. Zangwill LM, Jain S, Dirkes K, et al. The rate of structural change: the confocal scanning laser ophthalmoscopy ancillary study to the ocular hypertension treatment study. *Am J Ophthalmol* 2013;155(6):971–982.
10. Fortune B. Pulling and tugging on the retina: mechanical impact of glaucoma beyond the optic nerve head. *Invest Ophthalmol Vis Sci* 2019;60(1):26–35.
11. Chauhan BC, Danthurebandara VM, Sharpe GP, et al. Bruch's membrane opening minimum rim width and retinal nerve fiber layer thickness in a normal white population: a multicenter study. *Ophthalmology* 2015;122(9):1786–1794.
12. Luo H, Yang H, Gardiner SK, et al. Factors influencing central lamina cribrosa depth: a multicenter study. *Invest Ophthalmol Vis Sci* 2018;59(6):2357–2370.
13. Gardiner SK, Boey PY, Yang H, Fortune B, Burgoyne CF, Demirel S. Structural measurements for monitoring change in glaucoma: comparing retinal nerve fiber layer thickness with minimum rim width and area. *Invest Ophthalmol Vis Sci* 2015;56(11):6886–6891.
14. Mansberger SL, Menda SA, Fortune BA, Gardiner SK, Demirel S. Automated segmentation errors when using optical coherence tomography to measure retinal nerve fiber layer thickness in glaucoma. *Am J Ophthalmol* 2017;174:1–8.
15. Gardiner SK, Ren R, Yang H, Fortune B, Burgoyne CF, Demirel S. A method to estimate the amount of neuroretinal rim tissue in glaucoma: comparison with current methods for measuring rim area. *Am J Ophthalmol* 2014;157(3):540–549.e2.
16. Hogan MJ, Alvarado JA, Weddell JE. Histology of the Human Eye. Philadelphia, PA: Saunders; 1971.
17. Kiumehr S, Park SC, Syril D, et al. In vivo evaluation of focal lamina cribrosa defects in glaucoma. *Arch Ophthalmol* 2012;130(5):552–559.
18. Tatham AJ, Miki A, Weinreb RN, Zangwill LM, Medeiros FA. Defects of the lamina cribrosa in eyes with localized retinal nerve fiber layer loss. *Ophthalmology* 2014;121(1):110–118.
19. Takayama K, Hangai M, Kimura Y, et al. Three-dimensional imaging of lamina cribrosa defects in glaucoma using swept-source optical coherence tomography. *Invest Ophthalmol Vis Sci* 2013;54(7):4798–4807.
20. Doyle E, Trivedi D, Good P, Scott RA, Kirkby GR. High-resolution optical coherence tomography demonstration of membranes spanning optic disc pits and colobomas. *Br J Ophthalmol* 2009;93(3):360–365.
21. Michalewski J, Michalewska Z, Nawrocki J. Spectral domain optical coherence tomography morphology in optic disc pit associated maculopathy. *Indian J Ophthalmol* 2014;62(7):777–781.
22. Nagesha CK, Ganne P. Occult optic disc pit maculopathy in a glaucomatous disc. *Middle East Afr J Ophthalmol* 2017;24(3):165–166.
23. Lee JH, Park HY, Baek J, Lee WK. Alterations of the lamina cribrosa are associated with peripapillary retinoschisis in glaucoma and pachychoroid spectrum disease. *Ophthalmology* 2016;123(10):2066–2076.
24. Fortune B, Reynaud J, Hardin C, Wang L, Sigal IA, Burgoyne CF. Experimental glaucoma causes optic nerve head neural rim tissue compression: a potentially important mechanism of axon injury. *Invest Ophthalmol Vis Sci* 2016;57(10):4403–4411.
25. Varma R, Spaeth GL, Hanau C, Steinmann WC, Feldman RM. Positional changes in the vasculature of the optic disk in glaucoma. *Am J Ophthalmol* 1987;104(5):457–464.
26. Wang B, Lucy KA, Schuman JS, et al. Location of the central retinal vessel trunk in the laminar and prelaminar tissue of healthy and glaucomatous eyes. *Sci Rep* 2017;7:9930.
27. Radcliffe NM, Smith SD, Syed ZA, et al. Retinal blood vessel positional shifts and glaucoma progression. *Ophthalmology* 2014;121(4):842–848.
28. Nagelhus EA, Veruki ML, Torp R, et al. Aquaporin-4 water channel protein in the rat retina and optic nerve: polarized expression in Muller cells and fibrous astrocytes. *J Neurosci* 1998;18(7):2506–2519.
29. Naka M, Kanamori A, Negi A, Nakamura M. Reduced expression of aquaporin-9 in rat optic nerve head and retina following elevated intraocular pressure. *Invest Ophthalmol Vis Sci* 2010;51(9):4618–4626.
30. Sun D, Qu J, Jakobs TC. Reversible reactivity by optic nerve astrocytes. *Glia* 2013;61(8):1218–1235.
31. Lye-Barthel M, Sun D, Jakobs TC. Morphology of astrocytes in a glaucomatous optic nerve. *Invest Ophthalmol Vis Sci* 2013;54(2):909–917.
32. Dai C, Khaw PT, Yin ZQ, Li D, Raisman G, Li Y. Structural basis of glaucoma: the fortified astrocytes of the optic nerve head are the target of raised intraocular pressure. *Glia* 2012;60(1):13–28.
33. Tehrani S, Johnson EC, Cepurna WO, Morrison JC. Astrocyte processes label for filamentous actin and reorient early within the optic nerve head in a rat glaucoma model. *Invest Ophthalmol Vis Sci* 2014;55(10):6945–6952.
34. Quillen S, Schaub J, Quigley H, Pease M, Korneva A, Kimball E. Astrocyte responses to experimental glaucoma in mouse optic nerve head. *PLoS One* 2020;15(8):e0238104.
35. Dibas A, Yang MH, He S, Bobich J, Yorio T. Changes in ocular aquaporin-4 (AQP4) expression following retinal injury. *Mol Vis* 2008;14:1770–1783.